Remote Sensing of Environment 173 (2016) 314–325

Contents lists available at ScienceDirect

Remote Sensing of Environment

journal homepage: www.elsevier.com/locate/rse

Full length article

A forest vulnerability index based on drought and high temperatures

David Mildrexler [a,*], Zhiqiang Yang [a], Warren B. Cohen [b], David M. Bell [b]

[a] Oregon State University, College of Forestry, Corvallis, OR, USA
[b] USDA Forest Service, Pacific Northwest Research Station, Corvallis, OR, USA

ARTICLE INFO

Article history:
Received 19 March 2015
Received in revised form 13 November 2015
Accepted 16 November 2015
Available online 28 November 2015

Keywords:
Forest vulnerability index
Stress, climate change
Drought
Aqua MODIS land surface temperature
Evapotranspiration
Water deficit

ABSTRACT

Increasing forest stress and tree mortality has been directly linked to combinations of drought and high temperatures. The climatic changes expected during the next decades – large increases in mean temperature, increased heat waves, and significant long-term regional drying in the western USA – will likely increase chronic forest stress and mortality. The aim of this research is to develop and apply a new forest vulnerability index (FVI) associated with drought and high temperatures across the Pacific Northwest region (PNW; Oregon and Washington) of the USA during the MODIS Aqua era (since 2003). Our technique incorporates the alterations to canopy water and energy exchange processes caused by drought and high temperatures with spatially continuous MODIS land surface temperature (LST) and evapotranspiration (ET), and with Parameter-elevation Relationships on Independent Slopes Model (PRISM) precipitation (P) data. With P and ET, we calculate a monthly water balance variable for each individual pixel normalized by forest type group (FTG), and then difference the water balance with the corresponding normalized monthly mean LST to calculate a monthly forest stress index (FSI). We then extract the pixel-specific (800-m resolution) statistically significant temporal trends of the FSI from 2003 to 2012 by month (April to October). The FVI is the slope of the monthly FSI across years, such that there is a FVI for each month. Statistically significant positive slopes indicate interannual increases in stress leading to expected forest vulnerability (positive FVI) for a given month. Positive FVI values were concentrated in the months of August and September, with peak vulnerability occurring at different times for different FTGs. Overall, increased vulnerability rates were the highest in drier FTGs such as Ponderosa Pine, Juniper, and Lodgepole Pine. Western Larch and Fir/Spruce/Mountain Hemlock groups occupy moister sites but also had relatively high proportion of positive FVI values. The Douglas-fir group had the second largest total area of increased vulnerability due to its large areal extent in the study area. Based on an analysis using imagery viewed in Google Earth, we confirm that areas with increased vulnerability are associated with greater amounts of stress and mortality. The FVI is a new way to conceptualize and monitor forest vulnerability based on first-order principles and has the potential to be generalized to other geographical areas.

1. Introduction

Terrestrial vegetation plays a critical role in water and energy cycles, with transpiration representing about 80 to 90% of terrestrial evapotranspiration (ET) and absorbing a tremendous amount of solar energy (Jasechko et al., 2013; Trenberth, Fasullo, & Kiehl, 2009). Since climate and the distribution of vegetation are so tightly linked (Mather & Yoshioka, 1968; Stephenson, 1990), plants are vulnerable to changes in precipitation, temperature, and related variables when those exceed species-specific physiological stress thresholds (Allen et al., 2010; IPCC, 2013; McDowell & Allen, 2015; Teskey et al., 2015). There is considerable uncertainty in how trees will cope with the rapid changes occurring in the climate system, including increasing global mean temperatures and a changing hydrologic cycle (Hartmann, Adams, Anderegg, Jansen, & Zeppel, 2015; IPCC, 2013; McDowell et al., 2008). The potential for broad-scale climate-induced forest die-off is of particular concern because of large carbon storage in forests, and their key role in providing a variety of other valuable ecosystem services (Breshears et al., 2005; Kurz, Stinson, Rampley, Dymond, & Neilson, 2008; McDowell & Allen, 2015; Millar & Stephenson, 2015; Smith et al., 2014). Urgently needed are remote sensing-based large-area forest stress and mortality detection and attribution techniques that can provide a priori assessments of forest status and trends, as in metrics that can be used to infer a measure of possible future harm (Allen, Breshears, & McDowell, 2015; Smith et al., 2014). Vulnerability metrics should have clear mechanistic links with remotely sensed metrics of vegetation that are sensitive to the changes in climate (Smith et al., 2014).

Globally, forests are showing signs of stress, such as reduced growth and leaf area decline, and increasing tree mortality that can be directly linked to combinations of drought and/or high temperatures (Allen et al., 2010; Anderegg, Kane, & Anderegg, 2013; Breshears et al., 2005;

* Corresponding author at: The Laboratory for Applications of Remote Sensing in Ecology, Department of Forest Ecosystems and Society, College of Forestry, Oregon State University, Corvallis, OR 97331, USA.
E-mail address: david.mildrexler@oregonstate.edu (D. Mildrexler).

http://dx.doi.org/10.1016/j.rse.2015.11.024
0034-4257/

Griffin & Anchukaitis, 2014; Martinez-Vilalta, Lloret, & Breshears, 2011; Pravalie, Sîrodoev, & Peptenatu, 2014; Allen et al., 2015; Vicente-Serrano et al., 2014; Steinkamp & Hickler, 2015). In western North America, climate change has been implicated in rapidly increasing background mortality rates during recent decades, with widespread die-offs affecting tree species across regions, environmental gradients, age and structure classes, and disturbance regimes (Breshears et al., 2005; van Mantgem et al., 2009; Vogelmann, Tolk, & Zhu, 2009; Williams et al., 2013). Broad-scale drivers of tree mortality known with high confidence, such as droughts that are hotter and more widespread due to continued warming, imply a future greater level of forest vulnerability, independent of the specifics of mortality mechanism (Allen et al., 2015). Higher rates of climate-induced tree mortality can cause major shifts in ecosystem structure and function (Allen & Breshears, 1998; Breshears et al., 2005) that have varied and long-term consequences on ecological communities (Anderegg et al., 2013; McDowell et al., 2008). Changes in forest structure and composition have important implications for availability and distribution of plant and animal habitat, especially in ecosystems dominated by one or a few foundational tree species (Ellison et al., 2005). Mortality events change the albedo and the latent and sensible heat fluxes, with feedbacks on regional climate (Anderson et al., 2011; Bonan, 2008; Chapin, Randerson, McGuire, Foley, & Field, 2008). Even when mortality is not realized, severe drought has long lasting effects on forests (Anderegg et al., 2015). A growing body of evidence in the literature indicates that there are physical signs of stress and decline that indicate an increased risk of tree mortality. The physical expression of forest stress associated with vulnerability may manifest initially as poor crown condition and/or a decline in leaf area (Dobbertin & Brand, 2001; Solberg, 2004) followed by a reduction in growth (Delucia, Maherali, & Carey, 2000; Pedersen, 1998; Suarez, Ghermandi, & Kitzberger, 2004), and then by the potential increase in susceptibility to insects and fire (Hicke et al., 2012; Westerling, Hidalgo, Cayan, & Swetnam, 2006). The exceptionally severe 2003 European drought produced widespread stress symptoms in many trees (premature leaf fall, yellowing, shedding) and resulted in a large number of weakened individuals (low radial growth and small amounts of stored carbohydrates) followed by increased mortality rates in 2004 and 2005 in areas where weather conditions remained unfavorable (Bréda, Huc, Granier, & Dreyer, 2006). An index that relates climatic drivers of vulnerability directly to physiological stress factors would provide valuable information on forests that are predisposed to increased vulnerability.

Recent observational and experimental studies have highlighted the potential for warmer temperatures to compound the effects of severe drought events and exacerbate regional forest stress and die-off (Adams et al., 2009; Breshears et al., 2005; Griffin & Anchukaitis, 2014; van Mantgem et al., 2009; Williams et al., 2013). The increased energy load from warmer temperatures during severe drought events acts to heat and stress trees (Adams et al., 2009; Breshears et al., 2005; Stephenson, 1990). For example, the precipitation deficits of the 2012–2014 California drought were anonymously low, but not unprecedented. Yet record high temperatures could have exacerbated the drought by approximately 36%, resulting in the most severe drought conditions in over a century of instrumental observations (Griffin & Anchukaitis, 2014). In the southwestern US (SWUS) increasing warm-season vapor pressure deficit (largely controlled by the maximum daily temperature) was found to be the primary driver of an ongoing forest drought-stress event that is more severe than any event since the late 1500s megadrought (Williams et al., 2013). The strong correspondence between temperature-driven forest drought-stress and tree mortality, combined with the relatively high confidence in the projections of continued warming in the SWUS, portends future intensified forest drought stress and increased forest decline (Williams et al., 2013). In a study that estimated vulnerability of 15 tree species in the western USA and Canada to significantly warmed climate conditions, 30% of the species recorded ranges were deemed vulnerable based on the majority of years being unsuitable for the species (Coops & Waring, 2011). Projections for the western USA indicate that far greater chronic forest stress and mortality risk should be expected in coming decades due to the large increases in mean temperature and significant long-term regional drying, as well as the frequency and severity of extreme droughts and heat waves (Allen et al., 2015; Cook, Smerdon, Seager, & Coats, 2014; IPCC, 2013; Jentsch, Kreyling, & Beierkuhnlein, 2007; Moritz et al., 2012). Urgently needed is a remote sensing-based forest vulnerability index (FVI) that explicitly tracks where and when forests are becoming increasingly vulnerable to drought and increased temperature stress, to assess potential climate change impacts on vegetation and associated feedbacks to the climate system (Allen et al., 2015; McDowell et al., 2008; Smith et al., 2014).

The majority of vulnerability assessments derived from spaceborne data are conducted a posteriori, such that the disturbances (e.g., drought, wildfire, hurricane) had to occur prior to research being conducted (Smith et al., 2014). Global drought monitoring approaches such as the widely applied Vegetation Temperature Condition Index and the more recently developed Global Terrestrial Drought Severity Index have proven effective at providing information on the extent and severity of drought events (Kogan, 1997; Mu, Zhao, Kimball, McDowell, & Running, 2013). However, these metrics do not track longer term (multiple years to decades) forest stress trends, and lack the ability to deliver a priori information regarding where vegetation is likely becoming increasingly vulnerable to drought and increased temperature stress. An FVI at spatial and temporal scales relevant to land management that could be regularly updated would provide managers with knowledge of where and when forests are under multi-year stress so that proactive remedial actions could be better prioritized to have the greatest effect (Millar & Stephenson, 2015; Smith et al., 2014). Our objectives are to: 1) Develop an FVI that detects where and during which month of the growing season (April through October) forests are likely becoming increasingly vulnerable to climate-induced physiological stress associated with drought and high temperatures, and maps vulnerability across the Pacific Northwest region (PNW; Oregon and Washington) of the USA. 2) Understand the behavior of the FVI relative to its driving factors.

2. Land surface temperature and the biophysical link to plant canopy stress

Climatological data can be developed for two kinds of surface temperatures: near-surface air temperature (T_{air}) and land surface temperature (LST) (Jin & Dickinson, 2010). T_{air} is measured 1.5 m above the ground level at official weather stations with sensors protected from radiation and adequately ventilated (Karl, Miller, & Murray, 2006). Many standard drought monitoring indices, such as the Palmer drought severity index (PDSI), rely on T_{air} from the weather station network. The inequitable distribution of weather stations over the global land surface and the lack of information in areas with sparse or no stations limit the drought monitoring capability and the spatial resolution of the output products based on T_{air} data (Daly et al., 2008; Kogan, 1997; Mu et al., 2007; Mu et al., 2013). Although correlated with T_{air}, LST differs from T_{air} in its physical meaning, magnitude, and measurement techniques (Jin & Dickinson, 2010). LST can be estimated from measurements of thermal radiance coming from the land surface, retrieved from satellite, and mapped globally. LST from the Moderate Resolution Imaging Spectroradiometer (MODIS) measures the canopy foliage temperature in vegetated areas, a unique and useful ecological parameter because critical temperature dependent physiological processes and associated energy fluxes occur in the vegetated canopy. A global analysis of the relationship between remotely sensed annual maximum LST from the Aqua MODIS sensor and the corresponding site-based maximum air temperature for every World Meteorological Organization station on Earth showed that LST is more tightly coupled to the radiative and

thermodynamic characteristics of the Earth's surface (Mildrexler, Zhao, & Running, 2011a). LST is more sensitive to changes in vegetation density compared to T_{air} and captures additional information on the biophysical controls on surface temperature, such as surface roughness and transpirational cooling (Mildrexler et al., 2011a). We use LST rather than T_{air} to emphasize the direct thermal response of rising leaf temperatures and plant moisture stress associated with drought and increasing temperatures in the FVI.

3. The FVI and its conceptual foundation

We developed a conceptual model to demonstrate the multi-year interactions of LST and water balance (WB) to developing forest stress and increasing vulnerability (Fig. 1). WB, calculated as precipitation minus ET (P-ET) and commonly used to represent regional water balance (Mu, Jones, Kimball, McDonald, & Running, 2009; Swenson & Wahr, 2006; Zhang et al., 2009), is the net flux of water between the atmosphere and the biosphere. At the monthly timestep, P-ET provides a measure of the water surplus or deficit for the analyzed month. We refer to a positive WB (precipitation exceeds evaporative demand) as a *water surplus*, and a negative WB (evaporative demand exceeds precipitation) as a *water deficit*. During a water deficit, soil drying is occurring, and there is less water available for plants to transpire into the atmosphere. Changes in transpiration (latent heat flux) are directly coupled to leaf temperature such that an increase in canopy foliage temperature at otherwise similar environmental conditions indicates reduced transpiration (Jones, 1999; Scherrer, Bader, & Korner, 2011). Thus LST and WB generally have an inverse relationship whereby LST increases and peaks around mid-summer, commensurate with an increasing water deficit in the study area (Fig. 1). The pixel-specific monthly differences between normalized LST and WB result in a forest stress index (FSI) computed at monthly intervals over the growing season. In spring during low water stress conditions, forests dissipate incoming shortwave solar radiation efficiently through partitioning to the latent heat flux (LE) associated with transpiration, and thereby maintain canopy temperatures close to that of the surrounding air temperatures (Mildrexler, Zhao, & Running, 2011a; Nemani & Running, 1997). The FSI value associated with a water surplus and low thermal stress is low. In summer, increasing thermal and/or water stress has the effect of lowering midday transpiration and the associated LE (Manzoni, Vico, Porporato, & Katul, 2013). The increased partitioning of solar energy to the sensible heat flux results in a thermal response of rising leaf temperatures (Scherrer et al., 2011) and higher FSI values. The FSI peaks in July and August due to high temperatures and water deficits.

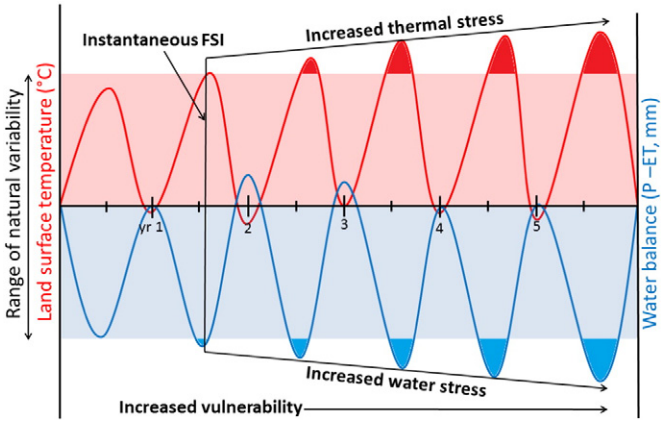

Fig. 1. Conceptual model for the FVI, showing annual fluctuations in LST and WB for a hypothetical land area (or pixel) through time. As the water deficit increases during drought (increased water stress), LST also increases beyond the range of natural variability (increased thermal stress).The FSI is an instantaneous measure of the difference between normalized LST and WB variables. The FVI translates the increasing FSI values across time into increasing vulnerability.

During a multi-year drought event, thermal and water stress intensify across years resulting in interannual increases in the FSI values. Increasing FSI values for a given month across years translate into areas of increasing vulnerability detected by the FVI.

We demonstrated the conceptual model at the previously established Oregon Transect Ecosystem Research project sites, which cover much of the broad climate and biomass gradient found in the north-temperate zone (Peterson & Waring, 1994), particularly in the west (sites indicated by black stars on Fig. 3). Monthly LST and WB data (described in Section 4.2) from a three by three 800-m grid centered on the six sites (Peterson & Waring, 1994) were plotted against each other as in the conceptualized model behavior to evaluate the LST and WB relationship (Fig. 2). The relationship supports the behavior of LST and WB conceptualized in the FVI model (Fig. 1) over the large temperature-moisture gradient and major vegetation zones sampled along the transect (Fig. 2). For example, at all six sites LST peaked around mid-summer commensurate with the largest water deficit reflecting the hot dry summers that characterize the PNW region (Fig. 2). The magnitude of these fluctuations varied from the coastal forests (site 1) with relatively low summer LST and large annual WB fluctuations, to juniper forest in the high desert (site 6) with high summer LST and only minor fluctuations in WB due to the lack of rainfall. Higher mid-summer LST values were evident in the drier forest types located within the rainshadow of the Cascades Mountain Range (sites 5 and 6), and in the High Cascades due to high elevation (site 4). Mid-summer LST values were also relatively high and WB fluctuations dampened at site 2 owing to the rainshadow effect of the Coastal Mountain Range. The LST and WB (P-ET) terms used to develop the FVI closely track the dynamics of the climatic factors that limit vegetation growth in the PNW (temperature and water) (Churkina & Running, 1998; Nemani & Running, 2003).

4. Data and methods

4.1. Study area

The PNW region of the USA (Oregon and Washington) covers a broad range of forest types and associated (level 3) ecoregions (Fig. 3; Omernik, 1987). This study focuses on forests, and relies on a Forest Type Groups (FTG) map of the United States dataset developed by Ruefenacht et al. (2008). The maritime influence is strong in the Coast Range, West Cascades, Puget Lowland, and North Cascades, and thus these ecoregions contain moist FTGs such as Hemlock/Sitka Spruce, Douglas-fir, Fir/Spruce/Mountain Hemlock, and Alder/Maple (Fig. 3). The Eastern Cascades, Northern Rockies, and Blue Mountains ecoregions are in the rain shadow of the Cascades Mountains and thus harbor drier FTGs including Ponderosa Pine, Western Larch, Juniper, and drier Douglas-fir (Fig. 3). Fir/Spruce/Mountain Hemlock and Lodgepole Pine are present at higher elevations in eastside ecoregions. The forests of the Klamath Mountains are primarily classified as within the Douglas-fir FTG, but Ponderosa Pine, White Pine, and Western Oak is present. While the precipitation and temperature regimes and associated forest types vary substantially across the study area, the region shares a common climatic feature of little precipitation in summer months. This low summer precipitation pattern results in typical dry conditions conducive to droughts (Bumbaco & Mote, 2010).

4.2. Datasets used to calculate the FVI

We utilize three datasets to map forest vulnerability due to drought and high temperatures across the study area; MODIS LST, MODIS ET, and Parameter-elevation Relationships on Independent Slopes Model (PRISM) Precipitation. These datasets provide systematic and continuous spatial information needed to develop repeatable, quantitative long-term measures of forest vulnerability for large areas.

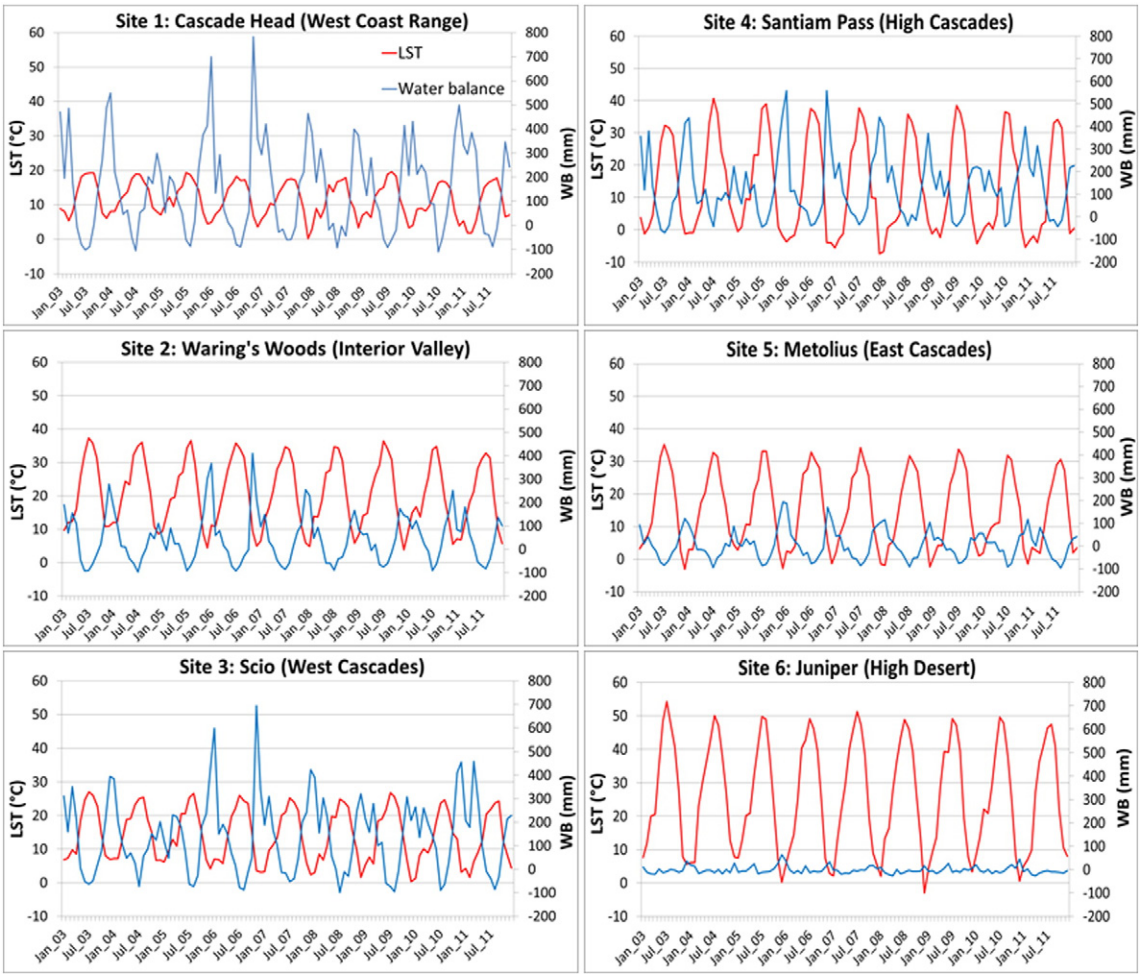

Fig. 2. LST and WB datasets across the Oregon Transect support the FVI conceptual model (Fig. 1) and reflect the different climatic regimes and major vegetation zones sampled along this large temperature–moisture gradient. Major vegetation zones: Site 1: Sitka Spruce; Site 2: Douglas-fir; Site 3: Douglas-fir; Site 4: Subalpine; Site 5: Ponderosa Pine; Site 6: Juniper.

4.2.1. Aqua MODIS land surface temperature (LST)

Two MODIS instruments, Terra and Aqua, monitor the Earth's LST as derived from the thermal-infrared (TIR) radiation emitted by the land surface (Wan & Li, 1997). The first MODIS instrument on the Terra platform was launched on December 18, 1999 and the second MODIS instrument on the Aqua platform was launched on May 4, 2002. The strengths of the MODIS instruments include continuous spatial coverage, high geolocation accuracy, high radiometric resolution, and accurate calibration in the visible, near-infrared and TIR bands (Wan, Zhang, Zhang, & Li, 2004). MODIS LST data provides 1-km surface temperature measurements from clear-sky pixels retrieved from brightness temperatures in bands 31 and 32 with the generalized split-window algorithm (Wan & Dozier, 1996). LST from the Aqua MODIS sensor was chosen for this study because of Aqua's afternoon overpass time of approximately 1:30 pm, close to the maximum temperature of the land surface. Measurements close to the high temperature peak of diurnal fluctuation better reflect the thermal response of rising leaf temperatures due to decreased LE as stomata close, and soil litter surfaces dry, accentuating differences in LST among vegetation cover types (Mildrexler et al., 2011a). As a result, it is more suitable for some regional and global change studies and is particularly well-suited for investigations of drought-induced thermal stress (Wan, Wang, & Li, 2004; Wan, Zhang, et al., 2004). The high-quality satellite-derived LST datasets from MODIS are currently used for a variety of applications including large-scale ecosystem disturbance detection (Coops, Wulder, & Iwanicka, 2009; Mildrexler, Zhao, & Running, 2009), drought monitoring (Wan, Wang, et al., 2004), land cover monitoring (Julien & Sobrino, 2008), agro-meteorology studies (Anderson, Norman, Mecikalski, Otkin, & Kustas, 2007), biodiversity studies (Albright et al., 2011), biophysical studies (Li et al., 2015), and have been proposed as an integrative global change metric (Mildrexler et al., 2011b). We derived monthly mean LST from the 1-km 8-day Aqua MODIS LST (MYD11A2) data for further analysis.

4.2.2. MODIS evapotranspiration (ET)

The MODIS ET (MOD16A2) data provides 1-km terrestrial modeled total evapotranspiration estimates at monthly intervals in mm/month for calculations of water and energy balance (Mu, Zhao, & Running, 2011). The ET algorithm uses a Penman-Monteith approach driven by MODIS land cover, albedo, leaf area index (LAI) and Enhanced Vegetation Index, and daily surface meteorological inputs (Mu et al., 2011). Terrestrial ET includes evaporation from wet and moist soil, from rainwater intercepted by the canopy before it reaches the ground, and the transpiration through stomata on plant leaves and stems. MODIS ET was used to quantify the effects of land-use change associated with sugar-cane expansion on climate in the Brazilian Cerrado (Loarie, Lobell, Asner, Mu, & Field, 2011), and the effects of afforestation on climate at high latitudes (Montenegro et al., 2009). The biophysical effects of global forest cover changes were examined using MODIS ET and other remote sensing datasets (Li et al., 2015). The MODIS ET is a key input in the Global Drought Severity Index (Mu et al., 2013) and has been used

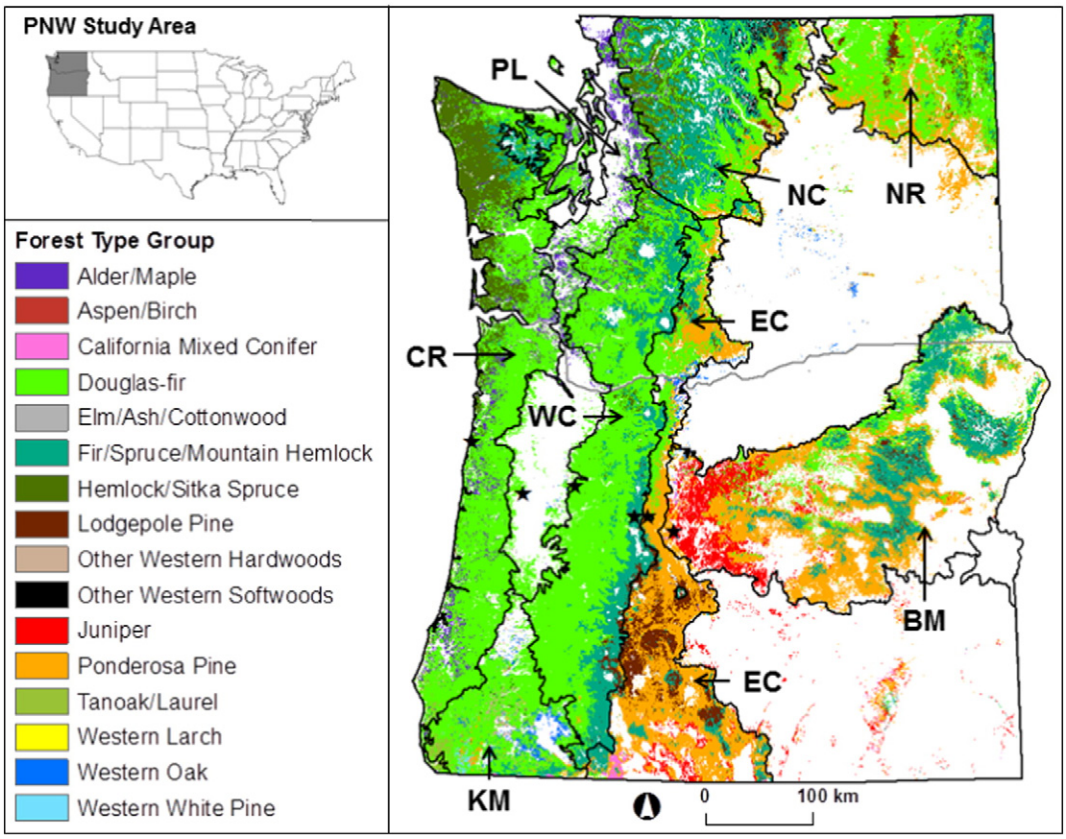

Fig. 3. Study area (PNW; the States of Washington and Oregon, USA) showing the locations of each FTG and Level 3 Ecoregion boundaries (black lines) from Omernik (1987). Spatial distribution of FTGs reflects the dominant west-to-east moisture gradient resulting in drier FTGs (Ponderosa Pine, Juniper) in the east part of the study area. Ecoregion abbreviations: CR: Coast Range; WC: West Cascades; EC: East Cascades; NC: North Cascades; NR: Northern Rockies; BM: Blue Mountains; KM: Klamath Mountains; PL: Puget Lowland. Black stars indicate location of Oregon Transect sites evaluated in Fig. 2.

to assess spatial and seasonal patterns in ET across the pan-Arctic domain (Mu et al., 2009).

4.2.3. PRISM precipitation (P)

The PRISM data provides 800-m resolution total monthly precipitation (rain plus melted snow) in mm/month (Daly et al., 2008). The dataset is a spatial interpolation between observational surface stations. PRISM calculates a climate–elevation regression for each digital elevation model (DEM) grid cell, and stations entering the regression are assigned weights based primarily on the physiographic similarity of the station to the grid cell (Daly et al., 2008). The PRISM method accounts for the major physiographic factors influencing climate patterns at scales of 1 km and greater and are the most accurate representation of the spatial climate patterns in the western USA (Daly et al., 2008). The PRISM datasets have been widely used in climatic and ecosystem response studies (http://www.prism.oregonstate.edu/documents/).

4.3. Input datasets and uncertainties

The MODIS LST products have been validated within 1 K at multiple sites in relatively wide ranges of surface and atmospheric conditions (Wan, 2008; Wan, Zhang, et al., 2004). Refinements to the Version 5 LST product have minimized the main sources of uncertainty caused by cloud contamination and in accurately estimating the surface emissivity, and significantly improved the accuracy and stability of the MODIS LST products (Wan, 2008). For uniform land surfaces with known spectral emissivity characteristics, the uncertainty in LST retrieved by the generalized split-window algorithm could be equal to or smaller than 0.5 K (Wan & Dozier, 1989; Li & Becker, 1993). Since emissivity is well-known for dense evergreen canopies, our focus on the evergreen dominated forests of the PNW helps minimize uncertainty in the LST product (Wan & Li, 1997).

Uncertainty in the MODIS ET data primarily arises from input data sources and algorithm limitations (Mu et al., 2011). The MODIS product inputs and daily surface meteorological inputs can introduce biases to ET estimates that are difficult to detect (Mu et al., 2011). Algorithm limitations are in part due to the large number of physical factors involved in soil surface evaporation and plant transpiration processes. The MODIS ET product used in this study is based on an improved ET algorithm. An examination of the new ET product at 46 AmeriFlux eddy covariance flux towers showed that the improved algorithm estimates capture the magnitudes of the ET measurements better than the old ones, reducing the tower-specific mean absolute error of the daily ET from 0.39 mm day^{-1} with the old algorithm to 0.33 mm day^{-1} (Mu et al., 2011). For an in-depth discussion of MOD16 ET see Mu et al. (2011).

Estimating uncertainty associated with the PRISM data is difficult because the true climate field is unknown, except at a relatively small number of observed points, which are themselves subject to measurement and siting uncertainties (i.e. relocations, changes in instrumentation and/or exposure, effects of land-use change, and changing observing practices; Pielke et al., 2007), and are incorporated into the PRISM dataset itself (Daly et al., 2008). However, a comparison of PRISM with a dynamically downscaled weather model (Weather Research and Forecasting model (WRF)) of winter precipitation over complex terrain revealed that the two datasets provide a very similar overall map of precipitation, with only localized differences, demonstrating a level of model simulation skill that has heretofore been lacking (Gutmann et al., 2012). Comparison with WorldClim and Daymet datasets demonstrated the benefits of using a relatively dense station dataset, and the physiographically sensitive PRISM interpolations

process resulted in substantially improved climate grids over those of WorldClim and Daymet (Daly et al., 2008). Greatest improvements were in the mountainous and coastal areas of the western USA.

4.4. Forest vulnerability index (FVI)

The FVI is based on the FSI (Fig. 1) calculated at the pixel level for each month, from April through October, from the first full year of Aqua LST data (2003) through 2012. This seasonal period captures the primary physiologically active months for plants during which thermal and water stress tend to occur in our study region, and includes the onset and alleviation of these seasonal stress cycles. The ET and monthly mean LST were resampled using bilinear interpolation from 1-km to 800-m to match the precipitation resolution. The FTG data were resampled to 800-m using a majority rule and used as mask to isolate forests in the LST and WB datasets. To contrast LST and WB, as per our conceptual model, it was necessary to normalize those datasets, which was done at the FTG level. The normalized LST and WB were calculated as:

$$Z_i = \frac{y_i - \bar{y}}{SD_y} \quad (1)$$

where y_i is either the LST or WB for pixel i for a given month in a given year, and $\bar{y}$ and SD_y are the average and standard deviation of LST or WB, respectively, across months (April–October) and years (2003–2012). The FSI was calculated as

$$FSI = LSTz - WBz \quad (2)$$

where *FSI* is the forest stress index value computed, and *LSTz* and *WBz* are the normalized LST and WB, respectively.

The FVI describes the interannual trend (2003–2012) of the FSI, on a per month basis for each month from April to October, computed at the FTG level. FVI is the slope of the monthly values across years (Fig. 1), as calculated using ordinary least square regression. We chose a *p*-value of 0.1 to declare statistically significant positive or negative FVI slopes to evaluate vulnerability for this initial application, but any *p*-value could be chosen. This results in three general potential FVI outcomes for any given pixel on the landscape: a (1) positive or (2) negative statistically significant FVI slope, and (3) statistically insignificant slopes.

4.4.1. Filtering abrupt disturbances

Abrupt, higher intensity disturbances such as wildfires and harvesting can have significant effects on LST and WB, resulting in positive FVI values that are not of interest for this application. To mask these disturbances, the year and magnitude of abrupt disturbances (less than 4 years in duration) were mapped in this study using the Landsat-based detection of Trends in Disturbance and Recovery (LandTrendr) algorithm (Kennedy, Yang, & Cohen, 2010). We calculated the proportion of disturbed Landsat pixels, weighted by magnitude, within each 800-m pixel from 2000 to 2012. All pixels with weighted disturbance >30% were masked, following Sulla-Menashe et al. (2014). There is no FVI value associated with masked pixels.

4.5. Understanding FVI behavior in relation to driving factors

To understand the behavior of the FVI in relation to LSTz and WBz, we computed the slopes of the monthly FSI components, LSTz and WBz, as was done to calculate the FVI from the monthly FSI values. To determine the upper and lower thresholds for mapping the LSTz and WBz consistently across months, positive and negative slopes were separated for each month. For pixels having statistically significant FVI values (both positive and negative), the corresponding LSTz and WBz slopes were extracted and ranked separately for the positive (ascending) and negative (descending) slopes. Once ranked, the values that correspond to the 95th percentile from the zero point were found for each set of positive and negative slopes for each month. The maximum (positive slopes) and minimum (negative slopes) of the 95th percentile values were then applied to map the scale range for each month.

4.6. Linking the FVI to observable stress and mortality

Connecting the FVI to the physical expression of vulnerability, such as reduction in leaf area, growth decline, and mortality is a critical step that needs to be explored in detail. For this initial application, we chose to look for direct visual evidence of canopy die-off and mortality in association with positive FVI areas in Google Earth. A random sample of 132 points was established across Oregon and Washington in forest areas not impacted by abrupt disturbances. At each point, the corresponding 800-m FVI pixel boundary was extracted and imported into Google Earth for visual interpretation. Then, using the time series of high resolution Google Earth images over the study period, presence of stress and mortality (dead and dying trees) was recorded at each plot based on visual interpretation. Pixels that contained widespread canopy die-off and/or mortality, indicated by the presence of dead or dying trees spread across the pixel area, or that contained large patches of mortality, indicated by groups of adjacent dead or dying trees, were recorded as stressed. All other pixels were recorded as background mortality. Correspondingly, each pixels slope (FVI value) and *p-value* were extracted. Since the *p-value* declares a FVI value statistically significant, we plotted the proportion of observations labeled as stressed against *p-value*.

5. Results

5.1. FVI maps

From April to October, we see interesting trends in the FVI from 2003 to 2012 (Fig. 4, top panel). As per our conceptual model, positive FVI values (*p-value* < 0.1) denote increased vulnerability. Negative values, although not explicitly considered in our conceptual model, do have potentially important implications (see Section 6). Close examination reveals that positive FVI values do not appear until the month of July, and are few and scattered in the southern Blue Mountains and southern East Cascades ecoregions. In August large patches of increased vulnerability emerge in the Blue Mountains, East Cascades, West Cascades, and Klamath Mountains. Positive FVI values can be found in every ecoregion in the study area during August. Additionally, August is a major transition period for the trajectory of the FVI values and thus had the most mixed patterns of positive and negative FVI values of any month (Fig. 4). Area experiencing increased vulnerability peaked in September and was most prevalent in the relatively dry Northern Rockies, East Cascades and Blue Mountains ecoregions, but was also widespread in the Oregon portion of the Coast Range and West Cascades. The Blue Mountains are notable for their concentration of area with increased vulnerability in the southeast and northeast portions of the ecoregion in September. Interestingly, the large patches with positive FVI in August did not persist through September. In October there were no positive FVI values.

The area covered by negative FVI increased from April through June. In April and May negative FVI values were limited to portions of the Coast Range, Puget Lowland, Cascades, and Northern Rockies. Then in June and July negative FVI was widespread across all forested ecoregions (Fig. 4). Only a small area was covered by negative FVI values during August, and these were essentially absent in September. In October areas of negative FVI again increased in all ecoregions except the Puget Lowland.

The large area of positive FVI values detected in central Oregon during August (Fig. 4) is associated with Juniper forests (Table 1). The proportion of the Juniper FTG with increased vulnerability was nearly threefold higher in August than in September (Table 1). California Mixed Conifer had the second highest proportion of area affected by

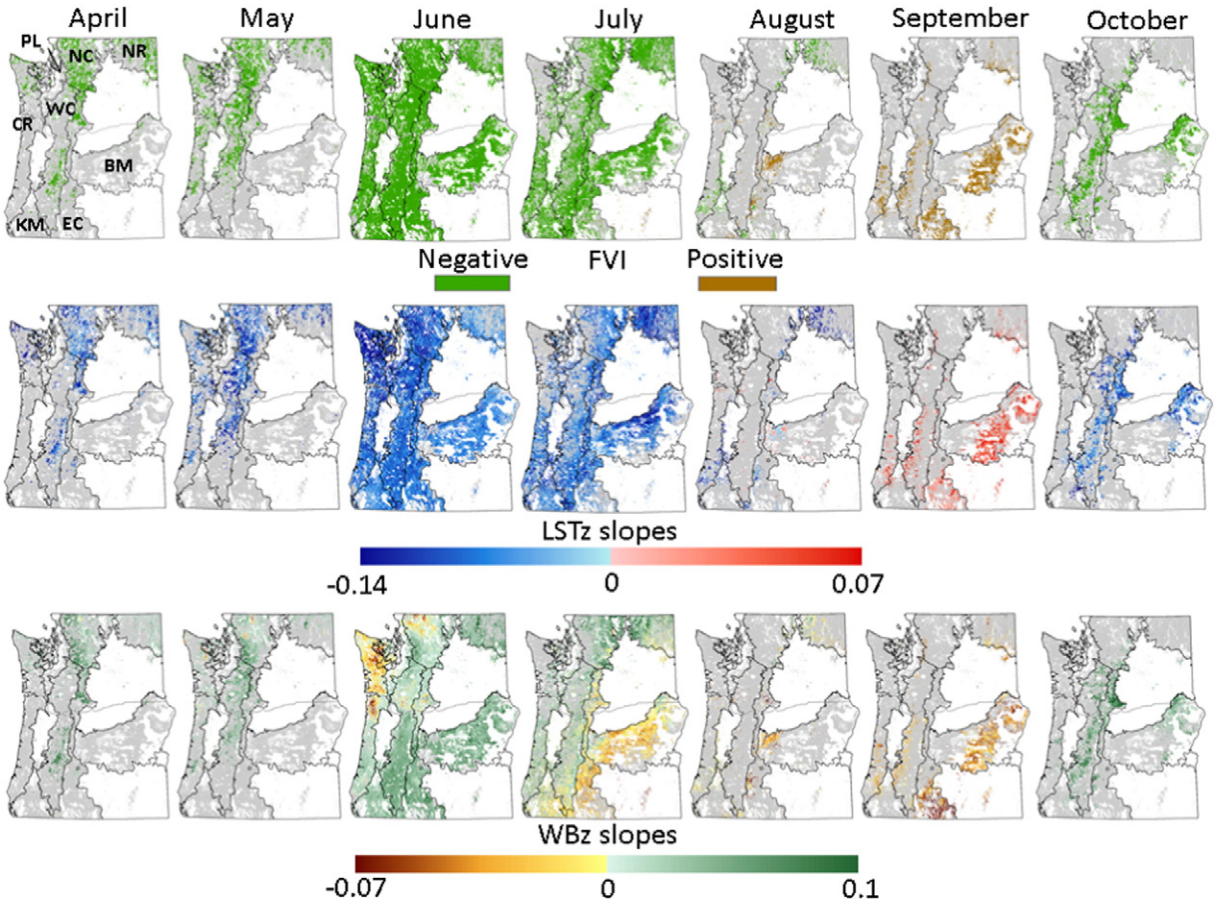

Fig. 4. FVI results for the forests of Oregon and Washington from 2003 to 2012, masked by significance (top panel; p-value <0.1). For simplification, all positive and negative values were collapsed into single classes. The slopes of LSTz (middle panel) and WBz (lower panel) for each month where positive or negative FVI values were detected illustrate the interactions that drive the FVI. The scale range corresponds to the global maximum (positive slopes) and global minimum (negative slopes) of the 95th percentile values from the zero point for each month.

increased vulnerability in August (12.3%), and a lesser amount in September, although not nearly as dramatic a decrease as for Juniper. Western Oak also had a greater proportion of positive FVI values in August than in September. However, for most FTGs the area of increased vulnerability peaked in September. For example, in the Ponderosa Pine FTG, the area of increased vulnerability went from 5% in August to 32.9% in September. Western Larch went from a very low positive FVI proportion in August, to the second highest in September (25.8%). Both of these FTGs are primarily located in the East Cascades, Blue Mountains, Northern Rockies, North Cascades, and are locally abundant in some areas of the Klamath Mountains ecoregions (Fig. 3). In the Douglas-fir FTG, the most important in terms of total areal coverage, the area of vulnerability increased substantially from August (1.1%) to September (7.6%). Hemlock/Sitka Spruce and Alder/Maple were least affected by increased vulnerability in August and September (less than 2%, Table 1), and these FTGs are concentrated within the moist Coast Range and Puget Lowland ecoregions. Lodgepole Pine and Fir/Spruce/Mountain Hemlock showed large increases in area affected by increased vulnerability from August to September. These FTGs tend to occupy higher elevations characterized by extreme annual climatic variations (Coops & Waring, 2011).

Table 1
The total area of each FTG, the area not impacted by abrupt disturbances and the proportion/area with positive FVI values relative to the area not impacted by abrupt disturbances during August and September (p-values <0.1).

	Total area	Area not abrupt disturbed	Positive FVI area			
			August		September	
Forest type group	(km^2)	(km^2)	(%)	(km^2)	(%)	(km^2)
Juniper	7127	7060	29.0	2047	10.4	733
Douglas-fir	104,988	98,993	1.1	1093	7.6	7544
Ponderosa Pine	41,551	39,827	5.0	1998	32.9	13,084
Western White Pine	205	10.24	0.0	0	0.0	0
Fir/Spruce/Mountain Hemlock	36,797	35,163	0.9	324	14.6	5151
Lodgepole Pine	6917	6389	4.8	308	21.0	1340
Hemlock/Sitka Spruce	14,344	13,242	0.8	100	1.5	200
Western Larch	518	507	0.9	4	25.8	131
Other Western Softwoods	807	697	0.8	6	3.8	26
CA Mixed Conifer	673	657	12.3	81	10.0	66
Elm/Ash/Cottonwood	265	255	3.5	9	3.3	8
Aspen/Birch	63	63	2.0	1	7.1	4
Alder/Maple	7361	7119	0.2	14	1.4	99
Western Oak	1559	1430	4.7	68	0.7	10
Tanoak/Laurel	838	740	0.1	1	0.8	6
Other Western Hardwoods	671	659	1.9	13	1.8	12
Combined total	224,684	212,811		6066		28,413

5.2. Behavior of the FVI

The slopes of LSTz (middle panel) and WBz (lower panel) for each month where positive and negative FVI values were detected illustrate the interactions that drive the FVI (top panel) (Fig. 4). Areas experiencing negative FVI from April through October are highly consistent with areas experiencing decreasing interannual monthly temperatures (LSTz slopes). From April through July, area showing decreased temperatures in association with negative FVI increased from largely the North Cascades, Northern Rockies, and West Cascades to the whole study

region. In August, as temperature trends turn from decreasing to increasing, the first major areas of positive FVI values appear with increasing temperature trends in the western Blue Mountains and the southern East Cascades. In September, as positive FVI values surface fully, LSTz slopes are positive.

Trends in water balance (WBz slopes) follow generally similar trends in relation to FVI as trends in temperature, with some notable exceptions in June and July. In June, in the northwest part of the study area, especially the northern Coast Range and the northern part of the North Cascades, trends in water deficit were positive, even while trends in the remaining study area were largely in the opposite direction. Interestingly, locations where there has been a decreasing trend in WBz slopes are locations where there has also been a trend towards decreasing LSTz slopes, the combined effect of which has been towards negative FVI values, consistent across the study area more broadly. In July, we see decreasing WBz slopes across large areas of the east-southeast region of the study area, but little to no effect on the FVI turning positive, suggesting a need for tight coupling between trends in LST and WB to turn the FVI positive. August is interesting because while the areal extent with negative WBz slopes decreased across the east-southeast region, some locations where the Juniper type group experienced a positive FVI (Table 1) were affected more by negative trends in water balance than trends in temperature, a relative anomaly in this regard. In September, where we saw the most dramatic increases in FVI values, there was a tight coupling between trends in both driving variables.

5.3. FVI vs. stress and mortality observations

The comparison between the FVI and stress and mortality observed in Google Earth revealed that as *p-value* associated with FVI decreased, the proportion of stressed plots increased, confirming that positive FVI areas with very low *p-values* (high statistical significance) are associated with greater amounts of stress and mortality (Fig. 5). Below a *p-value* of 0.05 (dashed line) the proportion of stressed plots rapidly increased in association with these lower and more significant *p-values* (Fig. 5). Stressed plots were also present at higher *p-values*, although at lower proportions, possibly highlighting the limitations in directly linking an 800-m integrated pixel with visual observations of mortality in Google Earth.

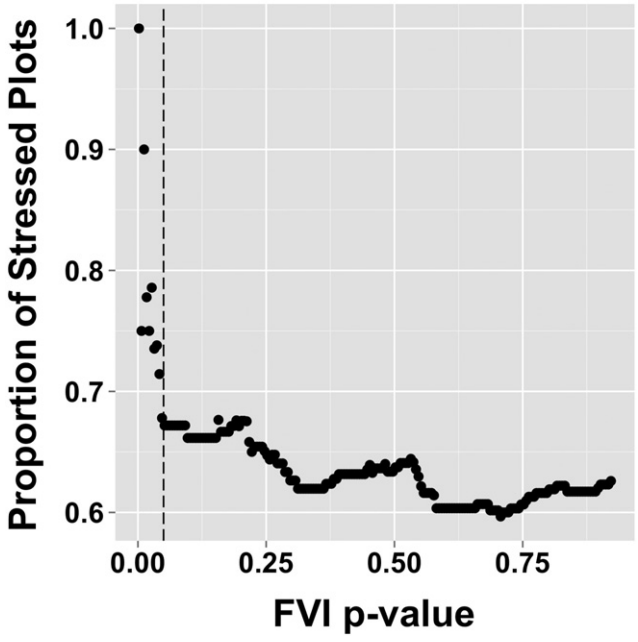

Fig. 5. The proportion of stressed plots, as observed in Google Earth, relative to changes in FVI statistical significance (p-value).

6. Discussion

A growing number of studies have linked forest stress and mortality to drought and increased temperature stress (van Mantgem et al., 2009; Breshears et al., 2005; Williams et al., 2013; Coops & Waring, 2011; Allen et al., 2010; Anderegg et al., 2013; Griffin & Anchukaitis, 2014; Martinez-Vilalta et al., 2011; Pravalie et al., 2014) highlighting the urgent need for metrics that can show where these changes are occurring (Allen et al., 2015; Smith et al., 2014). In response we developed and described in detail a new index, the FVI, for large-scale assessment of forest vulnerability to drought and high temperatures and applied it across the PNW region of the USA from 2003 to 2012. The FVI is based on a measure of instantaneous stress levels over the growing season, the FSI (Fig. 1). The conception of forest vulnerability as statistically significant trends in the FSI for each month across years is a potentially important new way to monitor forest vulnerability. The FVI characterizes interannual trends in the FSI, highlighting months where forest areas are experiencing longer-term increasing temperatures and water deficits, which does not coincide with the month of peak stress annually in our study region. The highest FSI values were detected during July (data not shown), but the FVI for July was largely decreasing, while the peak months for the FVI were in August and September (Fig. 4). It should be noted that negative trends in the WBz (WBz slopes) do not automatically translate to monthly WBz values that are negative. Even though there is a declining trend for a given month in the WBz values (a negative WBz slope), the values themselves can still be positive. This could be an important factor in why, even though there were negative WBz trends for large areas in June and July, slopes in temperature remained negative resulting in a negative FVI. Further study of the joint relationships of opposing temperature and water balance slopes, by FTG, is important, and could reveal some interesting physiological and/or biophysical setting that predisposes a given forest type to increasing vulnerability.

The FVI growing season monthly assessment across the PNW reveals a possible trajectory toward more extreme conditions indicated by negative FVI values in the spring, followed by a rapid transition to widespread positive FVI values that peak in August and September (Fig. 4), depending on forest type (Table 1). Positive FVI values tend to be associated with drier forest types and ecoregions. The proportion of a given FTG with positive FVI values generally increased from August to September, although there were a few notable exceptions that peaked in August (Juniper, California Mixed Conifer, and Western Oak). This indicates that peak vulnerability occurs at different times of the growing season for different FTGs, and there may be different sensitivities to the types relative to the others with respect to the driving variables. The normalization of LST and WB by FTG was critical for elucidating these FTG-specific responses.

It is important to note that the monthly interval used in this study may not be ideal for capturing when peak FVI values occur. For example, it is possible that the second half of August and the first half of September are key periods, and that the arbitrarily defined monthly boundaries used here diminish some of the FVI signal. Furthermore, the timing of peak vulnerability will likely change outside of the study area because LST and WB relations will vary with local conditions. However, the conceptual approach, developed and tested here should be relevant as an indicator of increasing forest vulnerability to climate change more globally. Future work should explore how to fine-tune the analysis to better elucidate peak FVI periods and the dynamics of landscape transition periods where FVI values are shifting from negative to positive, such as observed here during July and August. Moreover, although negative FVI values were not explicitly considered in the conceptual development of the FVI, their emergence towards increasing areal importance leading up to August and September suggests that the PNW region is experiencing more extreme climate conditions from cooler and moister conditions in the fall, spring, and early summer months to warmer and

drier conditions in the mid- to late-summer months. The implication of this on the vegetation could be dramatic in the long term.

Peak vulnerability occurred during September for the majority of FTGs in this study (Table 1). In accordance with these findings field work in southwestern Oregon has shown that peak moisture stress usually occurs in September near the peak of drought (Waring, 1969). Close examination of the September FVI reveals important ecological patterns (Fig. 4). Large forested areas with positive FVI values were detected along semi-arid ecotones in the Northern Rockies, Blue Mountains, and Eastern Cascades ecoregions. Ecotonal shifts in vegetation distribution due to climate change are expected to be most rapid in semi-arid ecotones (Allen & Breshears, 1998). The drier FTGs that occupy the ecotonal boundaries also have the most positive FVI values, especially Ponderosa Pine in September and Juniper in August, but also Fir/Spruce/Mountain Hemlock in September (Table 1). Even in the relatively wet Puget Lowland, area of positive FVI was detected within the rain shadow of the Olympic Mountains. In agreement with previous research, our results indicate that increased vulnerability tends to be associated with drier conditions (Allen et al., 2010; Steinkamp & Hickler, 2015). But, even further, we have detected positive FVI values concentrated in the southern portions of the relatively moist Oregon Coast Range and West Cascades ecoregions. A latitudinally-induced hydrological gradient extends from relatively wet northwest Washington, to drier southwest Oregon. Within relatively moist ecoregions we found a potential increase in vulnerability associated with drier environments. Lending confidence to this finding is the fact that the FVI is computed specific to each FTG, accentuating differences along within class moisture gradients. Juniper and Western Oak type groups both peaked in August, and then showed relatively large decreases in their proportion with positive FVI values in September. The Juniper group occupies areas that receive very little annual precipitation and experience extreme summer drought (Fig. 2), whereas Western Oak occupy a broader range of climates in our study area, including lower elevations in the interior valleys characterized by hot, dry summer conditions. By September, these areas may be so dry that further increases in LST and water deficit do not occur. However, a drying trend in August, when some moisture is still available, may have resulted in the negative WBz slopes and mildly increased temperature trends driving the positive FVI (Fig. 4).

As seen in the PNW region, the FVI and its input variables are valuable for understanding how temperature and water balance patterns change and interact over the course of the growing season. Prior to the summer drought cycle, an interesting interaction occurs when the WBz slopes begin turning negative (July) earlier than the LSTz slopes (August) (Fig. 4). The negative LSTz slopes in July indicate that forests have access to groundwater enabling transpirational cooling of the canopy, an important factor in determining the negative FVI in July (Fig. 4). This suggests that future changes in the hydrologic cycle that affect the spring water balance could have important implications for water availability heading into the summer drought cycle in the PNW. These interacting changes include reductions in snowpack (Mote, Hamlet, Clark, & Lettenmaier, 2005), changes in the rain-snow transition zone (Klos, Link, & Abatzoglou, 2014), and changes in spring precipitation (Mote & Salathé, 2010). Changes that cause a shift toward negative WB trends earlier in the growing season will likely result in a commensurate earlier increase in LST trends, driving earlier positive FVI values. Some models project increases in spring precipitation in the PNW ranging from 3% to 8% (Mote & Salathé, 2010). Increasing spring rains could help to maintain positive water balance trends later into the growing season by replenishing soil moisture and buffering forests heading into the impending summer drought cycle (Bumbaco & Mote, 2010). These future WB and LST trends could have important effects on forest vulnerability in the PNW in the coming decades.

The interpretation of FVI significance in relation to *p-value* is critical. With only ten years of data for this initial application, we chose a *p-value* of 0.1 to maintain a relatively conservative threshold, but also to increase the expression of potentially ecologically important vulnerability patterns, beyond the more conventional 0.05 threshold. As we lengthen the data record, it is likely that some trends may reverse themselves over different time scales. We will need to consider the appropriate time scale to examine the trends in the FSI that drive the FVI. A temporal segmentation approach of the FSI (e.g., the LandTrendr algorithm, Kennedy et al., 2010) may help capture distinct trajectories that relate to FVI changes. Incorporating temporal segmentation into the analysis will also help minimize the effects of initial conditions which have leverage in context of regression on trend estimates. A drought event occurred in 2003, the first year of our study (Bumbaco & Mote, 2010). This resulted in relatively high FSI values in August and September. However, the landscape still has momentum in the positive FVI direction in many different ecoregions driven by warming (positive LSTz slopes) and drying trends (negative WBz slopes) once the full decade is considered (2003–2012) (Fig. 4). This indicates that the longer term increases in the FSI trend were not diminished by what can be considered conservative initial conditions. The August and September *p-value* maps show a large shift in the distribution of values across the landscape during those two months (Fig. 6). Adjusting the *p-value* would have a larger effect on the FVI in September than August due to the different distributions. However, for both months incremental *p-value* adjustments relative to the 0.1 threshold change the expression of FVI values mostly along the borders of positive FVI areas. Decreasing the *p-value* threshold to 0.05 would result in fewer positive FVI values during September, but the geographic pattern would remain similar with most positive values detected in the Northern Rockies, Blue Mountains, East Cascades, West Cascades, and Oregon Coast Range. Of related importance are the effects of abrupt disturbances on the FVI. The threshold used to filter abrupt disturbance can be changed to examine the effects of more conservative vs. more inclusive thresholds on forest vulnerability patterns. Lowering the threshold below the weighted 30% proportion used in this study would result in increased confidence of removing areas affected by relatively small disturbances, but may also increase errors of commission. Thresholds could also be determined for specific areas. For example, a lower threshold may be desirable in areas dominated by harvest, whereas a higher threshold may be better suited for areas primarily affected by large-scale natural disturbances. The ability to adjust the *p-value* and threshold used to filter abrupt disturbances give the FVI an interactive component that scientists or forest managers (or other users of FVI maps) can adjust for their own assessment needs.

The areas that the FVI identified as increasingly vulnerable to the effects of climate change are either likely to exhibit visible health and vigor effects in the immediate future or are already exhibiting those effects (Fig. 5). Vulnerability often differs by species and with changing environmental conditions. In our study area sensitivity to drought varies along an elevational gradient. Dry forests at relatively low elevations have high tolerance for drought, whereas high elevation forests have low tolerance for drought, and mid-elevation forests have medium tolerance (Haugo, Hall, Gray, Gonzalez, & Bakker, 2010). Climate change has increased the exposure of high and mid-elevation forests to drought and high temperatures and, consequently, increased mortality in these systems (Westerling et al., 2006). Therefore in our study area we expect that mortality rates should be more sensitive to increased positive FVI values in high elevation FTGs that exhibit limited drought tolerance (Fir/Spruce/Mountain Hemlock and Lodgepole Pine in Table 1). Conversely, drought tolerant species like Ponderosa Pine have adaptations to drought such as sparse canopies, deep rooting systems, and changes in biomass allocation, that balance reduced productivity in the short term with drought stress avoidance over the long term (Delucia et al., 2000; Williams, Law, Anthoni, & Unsworth, 2001). Therefore, increased stress associated with positive FVI may not as readily manifest as elevated mortality in drier portions of our study area (Haugo et al., 2010). Preliminary examination between the FVI and mortality measurements from the Forest Inventory and Analysis (FIA) plots across Oregon and Washington confirms this expectation (data not shown) and indicates

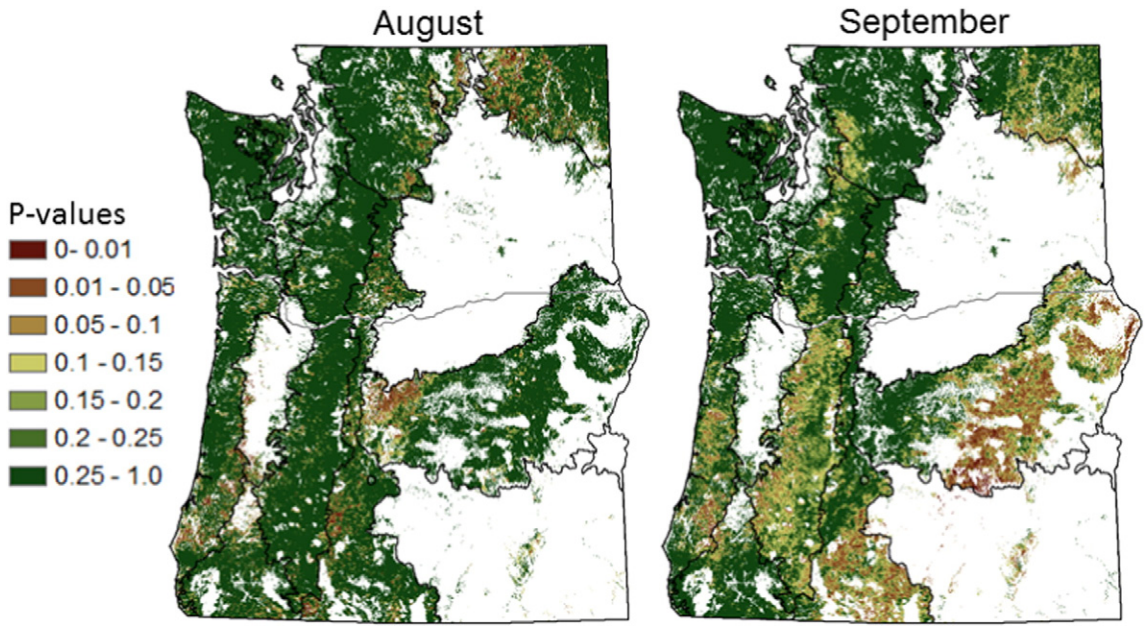

Fig. 6. P-values associated with FVI for August and September, 2003 to 2012.

a possible greater sensitivity of mortality to a high proportion of positive FVI in high (Fir/Spruce/Mountain Hemlock and Lodgepole Pine FTGs) and mid-elevation forests (Western Larch and Douglas-fir FTGs), relative to low elevation forests (Ponderosa Pine, Juniper, Tanoak/Laurel, and Western Oak). Calculating the FVI at the FTG level is essential for varying the interpretation of the FVI in relation to the different FTG tolerances for drought and high temperatures.

This paper has focused on the conceptual development and application of the FVI in response to the profound ecological and societal implications of global forest vulnerability to hotter drought (Allen et al., 2015; Joyce et al., 2014; Overpeck, 2013). The FVI is based on first principles relating canopy water and energy fluxes to changes in climate. We have shown that the FVI areas with low *p-values* (<0.05) are associated with greater amounts of mortality (Fig. 5). We now need to demonstrate the value of the FVI in relation to a more robust vulnerability signal (i.e. changes in canopy condition, leaf area, and growth rates). As increasingly hot and dry conditions cause reductions in leaf area (Dobbertin & Brand, 2001; Solberg, 2004), these changes will be commensurate with a reduction in ET and an increase in LST, thus changing the FVI. It is important to understand the sensitivity of the FVI to leaf area change, and to separate interannual variability in the plant communities LAI from steady reductions of leaf area over years (Delucia et al., 2000). Examining the LST and WB variables in isolation will help to elucidate the relationship between changes in leaf area, and the effects on the FVI. Hotter and drier conditions may also cause stomatal closure earlier in the growing season, invoking an earlier increase in LST, with possible feedbacks on vulnerability later in the growing season. These and other complex questions that integrate the timing of changing ecological responses reaffirm the need for products such as the FVI as inputs to empirical models (Allen et al., 2015). Moreover, it is necessary to link the FVI with ground-based measurements that record the visual health effects of the forest, structural and compositional states, and growth measurements to examine the relationship between the FVI, and changes in canopy condition and forest growth. The 800-m resolution of our region-wide vulnerability assessment presents a scale mismatch for directly linking the FVI to changes in forest canopy condition and/or growth rates associated with forest stress. To address this scale mismatch we are developing a framework that integrates the FVI with Landsat data, FIA data, and individual-tree models in an effort to link all the relevant scales that influence forest vulnerability. Landsat time series (LTS) data is promising due to its 30-m resolution and distinct spectral trajectories. Long, slow declines in the spectral trajectory of LTS data imply a slow and subtle process for forest change unfolding over many years (Kennedy et al., 2010). However, before meaningful comparisons can be made with the FVI, it is essential to characterize the relationship between the LTS spectral signature and declining canopy condition, just as was done for the LTS spectral trajectories associated with insect activity of varying duration and severity (Meigs, Kennedy, & Cohen, 2011).

7. Conclusions

We developed a FVI that identifies when and where forests have been experiencing increasingly high surface temperatures and greater growing season water deficits. Our method takes a direct approach to monitoring concurrent changes in canopy water and energy exchange processes that have clear mechanistic links to the effects of drought and high temperatures on vegetation (Fig. 1). By directly linking LST to WB for each month (April through October) across years (2003 through 2012), we have characterized how the monthly LST and WB trajectories change in relation to one another over the growing season to express the FVI. This has revealed that positive FVI slopes can result from multiple LST and WB slope combinations, such as occurred during August and September in the PNW (Fig. 4).

Ten years of observations from MODIS data are insufficient to establish long-term patterns or thresholds after which die-off might occur (Hilker et al., 2014). However, our results show a clear trend toward warmer and drier conditions in August and September across a variety of ecoregions and FTGs. If this trend continues, it portends increased forest stress and die-off in the PNW. With longer periods of observations we will be able to temporally segment these trends into periods of increasing and decreasing climate-induced stress, so that the FVI will serve as a monitoring tool for where and when different forest areas are vulnerable, and perhaps amenable to management intervention.

The FVI conceptual foundation is robust across one of the largest hydrological gradients in North America (Fig. 2) indicating that the metrics may be transferable to different ecosystems and larger areas, especially those characterized by a summer seasonal drought cycle. However, we emphasize that the WB and LST relations, and thus the joint influence on the FVI, will vary with local conditions. Examining the WB and LST relations in different areas, such as we did across the PNW (Fig. 2), is a

good starting point for conceptualizing the joint behavior of LST and WB in relation to the FVI.

Acknowledgments

This work was supported by the USDA Forest Service, Region 6 Climate Change Program, and the Graduate School and the Department of Forest Ecosystems and Society at Oregon State University. We thank Maosheng Zhao for providing the MODIS datasets and Robert Kennedy for use of the LandTrendr data.

References

Adams, H. D., Guardiola-Claramonte, M., Barron-Gafford, G. A., Villegas, J. C., Breshears, D. D., Zou, C. B., ... Huxman, T. E. (2009). Temperature sensitivity of drought-induced tree mortality portends increased regional die-off under global-change-type drought. *Proceedings of the National Academy of Sciences*, *106*, 7063–7066.

Albright, T. P., Pidgeon, A. M., Rittenhouse, C. D., Clayton, M. K., Flather, C. H., Culbert, P. D., & Radeloff, V. C. (2011). Heat waves measured with MODIS land surface temperature data predict changes in avian community structure. *Remote Sensing of Environment*, *115*, 245–254. http://dx.doi.org/10.1016/j.rse.2010.08.024.

Allen, C. D., & Breshears, D. D. (1998). Drought-induced shift of a forest-woodland ecotone: Rapid landscape response to climate variation. *Proceedings of the National Academy of Sciences*, *95*, 14839–14842.

Allen, C. D., Breshears, D. D., & McDowell, N. G. (2015). On underestimation of global vulnerability to tree mortality and forest die-off from hotter drought in the Anthropocene. *Ecosphere*, *6*(8), 129. http://dx.doi.org/10.1890/ES15-00203.1.

Allen, C. D., Macalady, A. K., Chenchouni, H., Bachelet, D., McDowell, N. G., Vennetier, M., ... Cobb, N. (2010). A global overview of drought and heat-induced tree mortality reveals emerging climate change risks for forests. *Forest Ecology and Management*, *259*, 660–684.

Anderegg, W. R. L., Kane, J., & Anderegg, L. D. L. (2013). Consequences of widespread tree mortality triggered by drought and temperature stress. *Nature Climate Change*, *3*, 30–36. http://dx.doi.org/10.1038/nclimate1635.

Anderegg, W. R. L., Schwalm, C., Biondi, F., Camarero, J. J., Koch, G., Litvak, M., ... Pacala, S. (2015). Pervasive drought legacies in forest ecosystems and their implications for carbon cycle models. *Science*, *349*, 528–532.

Anderson, M. C., Norman, J. M., Mecikalski, J. R., Otkin, J. A., & Kustas, W. P. (2007). A climatological study of evapotranspiration and moisture stress across the continental United States based on thermal remote sensing: 2. Surface moisture climatology. *Journal of Geophysical Research*, *112*. http://dx.doi.org/10.1029/2006JD007507.

Anderson, R. G., Canadell, J. G., Randerson, J., Jackson, R. B., Hungate, B. A., Baldocchi, D. D., ... O'Halloran, T. L. (2011). Biophysical considerations in forestry for climate protection. *Frontiers in Ecology and the Environment*, *9*, 174–182. http://dx.doi.org/10.1890/090179.

Bonan, G. B. (2008). Forests and climate change: Forcings, feedbacks, and the climate benefits of forests. *Science*, *320*, 1444–1449.

Bréda, N., Huc, R., Granier, A., & Dreyer, E. (2006). Temperate forest trees and stands under severe drought: A review of ecophysiological responses, adaptation processes and long-term consequences. *Annals of Forest Science*, *63*, 625–644.

Breshears, D. D., Cobb, N. S., Rich, P. M., Price, K. P., Allen, C. D., Balice, R. G., ... Meyer, C. W. (2005). Regional vegetation die-off in response to global-change type drought. *Proceedings of the National Academy of Sciences*, *102*(42), 15144–15148.

Bumbaco, K. A., & Mote, P. W. (2010). Three recent flavors of drought in the Pacific Northwest. *Journal of Applied Meteorology and Climatology*, *49*, 2058–2068. http://dx.doi.org/10.1175/2010JAMC 2423.1.

Chapin, F. S., III, Randerson, A. D., McGuire, A. D., Foley, J. A., & Field, C. B. (2008). Changing feedbacks in the climate–biosphere system. *Frontiers in Ecology and the Environment*, *6*, 313–320.

Churkina, G., & Running, S. W. (1998). Contrasting climatic controls on the estimated productivity of different biomes. *Ecosystems*, *1*, 206–215.

Cook, B. I., Smerdon, J. E., Seager, R., & Coats, S. (2014). Global warming and 21st century drying. *Climate Dynamics*, *43*, 2607–2627. http://dx.doi.org/10.1007/s00382-014-2075-y.

Coops, N. C., & Waring, R. H. (2011). Estimating the vulnerability of fifteen tree species under changing climate in Northwest North America. *Ecological Modelling*, *222*, 2119–2129.

Coops, N. C., Wulder, M. A., & Iwanicka, D. (2009). Large area monitoring with a MODIS-based disturbance index (DI) sensitive to annual seasonal variations. *Remote Sensing of Environment*, *113*, 1250–1261.

Daly, C., Halbleib, M., Smith, J. I., Gibson, W. P., Doggett, M. K., Taylor, G. H., ... Pasteris, P. P. (2008). Physiographically-sensitive mapping of temperature and precipitation across the conterminous United States. *International Journal of Climatology*, *28*(15), 2031–2064.

Delucia, E. H., Maherali, H., & Carey, E. V. (2000). Climatic-driven changes in biomass allocation in pines. *Global Change Biology*, *6*, 587–593.

Dobbertin, M., & Brand, P. (2001). Crown defoliation improves tree mortality models. *Forest Ecology and Management*, *141*, 271–284.

Ellison, A. M., Bank, M. S., Clinton, B. D., Colburn, E. A., Elliott, K., Ford, C. R., ... Webster, J. R. (2005). Loss of foundation species: Consequences for the structure and dynamics of forested ecosystems. *Frontiers in Ecology and the Environment*, *3*, 479–486.

Griffin, D., & Anchukaitis, K. J. (2014). How unusual is the 2012–2014 California drought? *Geophysical Research Letters*, *41*, 9017–9023. http://dx.doi.org/10.1002/2014GL062433.

Gutmann, E. D., Rasmussen, R. M., Liu, C., Ikeda, K., Gochis, D. J., Clark, M. P., ... Thompson, G. (2012). A comparison of statistical and dynamical downscaling of winter precipitation over complex terrain. *Journal of Climate*, *25*, 262–281. http://dx.doi.org/10.1175/2011JCLI4109.1.

Hartmann, H., Adams, H. D., Anderegg, W. R. L., Jansen, S., & Zeppel, M. J. B. (2015). Research frontiers in drought-induced tree mortality: Crossing scales and disciplines. *New Phytologist*, *205*, 965–969.

Haugo, R. D., Hall, S. A., Gray, E. M., Gonzalez, P., & Bakker, J. D. (2010). Influences of climate, fire, grazing, and logging on woody species composition along an elevational gradient in the eastern Cascades, Washington. *Forest Ecology and Management*, *260*, 2204–2213.

Hicke, J. A., Allen, C. D., Desai, A., Dietze, M. C., Hall, R. J., Hogg, E. H., ... Vogelmann, J. (2012). Effects of biotic disturbance on forest carbon cycling in the United States and Canada. *Global Change Biology*, *18*, 7–34.

Hilker, T., Lyapustin, A. I., Tucker, C. J., Hall, F. G., Myneni, R. B., Wang, Y., ... Sellers, P. J. (2014). Vegetation dynamics and rainfall sensitivity of the Amazon. *Proceedings of the National Academy of Sciences*, *111*(45), 16041–16046. http://dx.doi.org/10.1073/pnas.1404870111.

IPCC (2013). In T. F. Stocker, D. Qin, G. -K. Plattner, M. Tignor, S. K. Allen, J. Boschung, A. Nauels, Y. Xia, V. Bex, & P. M. Midgley (Eds.), *Working group I contribution to the IPCC fifth assessment report of the intergovernmental panel on climate change*. Cambridge, United Kingdom and New York, NY, USA: Cambridge university press. http://dx.doi.org/10.1017/CBO9781107415324 (1535 pp.).

Jasechko, S., Sharp, Z. D., Gibson, J. J., Birks, S. J., Yi, Y., & Fawcett, P. J. (2013). Terrestrial water fluxes dominated by transpiration. *Nature*, *496*, 347–351.

Jentsch, A., Kreyling, J., & Beierkuhnlein, C. (2007). A new generation of climate change experiments: Events, not trends. *Frontiers in Ecology and the Environment*, *5*, 365–374.

Jin, M., & Dickinson, R. E. (2010). Land surface skin temperature climatology: Benefitting from the strengths of satellite observations. *Environmental Research Letters*, *5*, 1–13. http://dx.doi.org/10.1088/1748-9326/5/4/044004.

Jones, H. G. (1999). Use of thermography for quantitative studies of spatial and temporal variation of stomatal conductance over leaf surfaces. *Plant Cell Environment*, *22*(9), 1043–1055.

Joyce, L. A., Running, S. W., Breshears, D. D., Dale, V. H., Malmsheimer, R. W., Sampson, R. N., ... Woodall, C. W. (2014). Ch. 7: Forests. In J. M. Melillo, T.(. T. C.). Richmond, & G. W. Yohe (Eds.), *Climate change impacts in the United States: The third national climate assessment* (pp. 175–194). U.S. Global Change Research Program. http://dx.doi.org/10.7930/J0Z60KZC.

Julien, Y., & Sobrino, J. A. (2008). The Yearly Land Cover Dynamics (YLCD) method: An analysis of global vegetation from NDVI and LST parameters. *Remote Sensing of Environment*, *113*, 329–334. http://dx.doi.org/10.1016/j.rse.2008.09.016.

Karl, T. R., Miller, C. D., & Murray, W. L. (2006). Temperature trends in the lower atmosphere: Steps for understanding and reconciling differences. In T. R. Karl, S. J. Hassol, C. D. Miller, & W. L. Murray (Eds.), *A report by the climate change science program and the subcommittee on global change research, Washington, DC*.

Kennedy, R. E., Yang, Z. G., & Cohen, W. B. (2010). Detecting trends in forest disturbance and recovery using yearly Landsat time series: 1. LandTrendr - Temporal segmentation algorithms. *Remote Sensing of Environment*, *114*, 2897–2910.

Klos, P. Z., Link, T. E., & Abatzoglou, J. T. (2014). Extent of the rain–snow transition zone in the western U.S. under historic and projected climate. *Geophysical Research Letters*, *41*, 4560–4568. http://dx.doi.org/10.1002/ 2014GL060500.

Kogan, F. N. (1997). Global drought watch from space. *Bulletin of the American Meteorological Society*, *78*, 621–636.

Kurz, W. A., Stinson, G., Rampley, G. J., Dymond, C. C., & Neilson, E. T. (2008). Risk of natural disturbances makes future contribution of Canada's forests to the global carbon cycle highly uncertain. *Proceedings of the National Academy of Sciences*, *105*, 1551–1555.

Li, Y., Zhao, M., Motesharrei, S., Mu, Q., Kalnay, E., & Li, S. (2015). Local cooling and warming effects of forests based on satellite observations. *Nature Communications*, *6*, 6603. http://dx.doi.org/10.1038/ncomms7603.

Li, Z. -L., & Becker, J. (1993). Feasibility of land surface temperature and emissivity determination from AVHRR data. *Remote Sensing of Environment*, *43*, 67–85.

Loarie, S. R., Lobell, D. B., Asner, G. P., Mu, Q., & Field, C. B. (2011). Direct impacts on local climate of sugar-cane expansion in Brazil. *Nature Climate Change*, *1*, 105–109.

van Mantgem, P. J., Stephenson, N. L., Byrne, J. C., Daniels, L. D., Franklin, J. F., Fule, P. Z., ... Veblen, T. T. (2009). Widespread increase of tree mortality rates in the western United States. *Science*, *323*, 521–524.

Manzoni, S., Vico, G., Porporato, A., & Katul, G. (2013). Biological constraints on water transport in the soil–plant–atmosphere system. *Advances in Water Resources*, *51*, 292–304. http://dx.doi.org/10.1016/j.advwatres.2012.03.016.

Martinez-Vilalta, J., Lloret, F., & Breshears, D. (2011). Drought-induced forest decline: Causes, scope and implications. *Biology Letters*, *8*, 689–691.

Mather, J. R., & Yoshioka, G. A. (1968). The role of climate in the distribution of vegetation. *Annals of the Association of American Geographers*, *58*, 29–41.

McDowell, N. G., & Allen, C. D. (2015). Darcy's law predicts widespread forest mortality under climate warming. *Nature Climate Change*, *5*, 669–672. http://dx.doi.org/10.1038/NCLIMATE2641.

McDowell, N. G., Pockman, W. T., Allen, C. D., Breshears, D. D., Cobb, N., Kolb, T., ... Yepez, E. A. (2008). Mechanisms of plant survival and mortality during drought: Why do some plants survive while others succumb to drought? *New Phytologist*, *178*, 719–739.

Meigs, G. W., Kennedy, R. E., & Cohen, W. B. (2011). A Landsat time series approach to characterize bark beetle and defoliator impacts on tree mortality and surface fuels in conifer forests. *Remote Sensing of Environment*, *115*, 3707–3718.

Mildrexler, D. J., Zhao, M., & Running, S. W. (2009). Testing a MODIS Global Disturbance Index across North America. *Remote Sensing of Environment*, *113*, 2103–2117.
Mildrexler, D. J., Zhao, M., & Running, S. W. (2011a). A global comparison between station air temperatures and MODIS land surface temperatures reveals the cooling role of forests. *Journal of Geophysical Research*, *116*, G03025. http://dx.doi.org/10.1029/2010JG001486.
Mildrexler, D. J., Zhao, M., & Running, S. W. (2011b). Satellite finds highest land skin temperatures on earth. *Bulletin of the American Meteorological Society*, *92*, 855–860.
Millar, C. I., & Stephenson, N. L. (2015). Temperature forest health in an era of emerging megadisturbance. *Science*, *349*, 823–826.
Montenegro, A., Eby, M., Mu, Q., Mulligan, M., Weaver, A. J., Wiebe, E. C., & Zhao, M. (2009). The net carbon drawdown of small scale afforestation from satellite observations. *Global and Planetary Change*, *69*, 195–204.
Moritz, M. A., Parisien, M. -A., Batllori, E., Krawchuk, M. A., Van Dorn, J., Ganz, D. J., & Hayhoe, K. (2012). Climate change and disruptions to global fire activity. *Ecosphere*, *3*(6), 1–22.
Mote, P. W., & Salathé, E. P., Jr. (2010). Future climate in the Pacific Northwest. *Climatic Change*. http://dx.doi.org/10.1007/ s10584-010-9848-z.
Mote, P. W., Hamlet, A. F., Clark, M. P., & Lettenmaier, D. P. (2005). Declining mountain snowpack in western North America. *Bulletin of the American Meteorological Society*, *86*, 39–49.
Mu, Q., Jones, L. A., Kimball, J. S., McDonald, K. C., & Running, S. W. (2009). Satellite assessment of land surface evapotranspiration for the pan-Arctic domain. *Water Resources Research*, *45*, W09420. http://dx.doi.org/10.1029/2008WR007189.
Mu, Q., Zhao, M., Heinsch, F. A., Liu, M., Tian, H., & Running, S. W. (2007). Evaluating water stress controls on primary production in biogeochemical and remote sensing based models. *Journal of Geophysical Research*, *112*, G01012.
Mu, Q., Zhao, M., Kimball, J. S., McDowell, N. G., & Running, S. W. (2013). A remotely sensed global terrestrial drought severity index. *Bulletin of the American Meteorological Society*, *94*, 83–98.
Mu, Q., Zhao, M., & Running, S. W. (2011). Improvements to a MODIS global terrestrial evapotranspiration algorithm. *Remote Sensing of Environment*, *115*, 1781–1800.
Nemani, R. R., & Running, S. W. (1997). Land cover characterization using multitemporal red, near-IR, and thermal-IR data from NOAA/AVHRR. *Ecological Applications*, *7*, 79–90.
Nemani, R. R., & Running, S. W. (2003). Climate-driven increases in global terrestrial net primary production from 1982 to 1999. *Science*, *300*, 1560–1563.
Omernik, J. M. (1987). Ecoregions of the conterminous United States. *Annals of the Association of American Geographers*, *77*, 118–125.
Overpeck, J. T. (2013). The challenge of hot drought. *Nature*, *503*, 350–351.
Pedersen, B. S. (1998). The role of stress in the mortality of Midwestern oaks as indicated by growth prior to death. *Ecology*, *79*, 79–93.
Peterson, D. L., & Waring, R. H. (1994). Overview of the Oregon transect ecosystem research project. *Ecological Applications*, *4*(2), 211–225.
Pielke, R. A., Sr., Davey, C. A., Niyogi, D., Steinweg-Woods, J., Hubbard, K., Lin, X., ... Blanken, P. (2007). Unresolved issues with the assessment of multidecadal global land surface temperature trends. *Journal of Geophysical Research*, *112*, D24S08. http://dx.doi.org/10.1029/2006JD008229.
Pravalie, R., Sîrodoev, I., & Peptenatu, D. (2014). Detecting climate change effects on forest ecosystems in southwestern Romania using Landsat TM NDVI data. *Journal of Geographical Science*, *24*, 815–832.
Ruefenacht, B., Finco, M. V., Nelson, M. D., Czaplewski, R., Helmer, E. H., Blackard, J. A., ... Winterberger, K. (2008). Conterminous U.S. and Alaska forest type mapping using forest inventory and analysis data. *Photogrammetric Engineering & Remote Sensing*, *74*(11), 1379–1388.
Scherrer, D. M., Bader, K. -F., & Korner, C. (2011). Drought-sensitivity ranking of deciduous tree species based on thermal imaging of forest canopies. *Agricultural Forest Meteorology*, *151*, 1632–1640.
Smith, A. M. S., Kolden, C. A., Tinkham, W. T., Talhelm, A. F., Marshall, J. D., Hudak, A. T., ... Gosz, J. R. (2014). Remote sensing the vulnerability of vegetation in natural terrestrial ecosystems. *Remote Sensing of Environment*, *154*, 322–337.
Solberg, S. (2004). Summer drought: A driver for crown condition and mortality of Norway spruce in Norway. *Forest Pathology*, *34*, 93–104.
Steinkamp, J., & Hickler, T. (2015). Is drought-induced forest dieback globally increasing? *Journal of Ecology*, *103*, 31–42.
Stephenson, N. (1990). Climatic control of vegetation distribution: The role of the water balance. *The American Naturalist*, *135*(5), 649–670.
Suarez, M. L., Ghermandi, L., & Kitzberger, T. (2004). Factors predisposing episodic drought-induced tree mortality in *Nothofagus*-site, climatic sensitivity and growth trends. *Journal of Ecology*, *92*, 954–966.
Sulla-Menashe, D., Kennedy, R. E., Yang, Z., Braaten, J., Krankina, O. N., & Friedl, M. A. (2014). Detecting forest disturbance in the Pacific Northwest from MODIS time series using temporal segmentation. *Remote Sensing of Environment*, *151*, 114–123.
Swenson, S., & Wahr, J. (2006). Estimating large-scale precipitation minus evapotranspiration from GRACE satellite gravity measurements. *Journal of Hydrometeorology*, *7*(2), 252–270. http://dx.doi.org/10.1175/JHM478.1.
Teskey, R., Wertin, T., Bauweraerts, I., Ameye, M., Mcguire, M. A., & Steppe, K. (2015). Responses of tree species to heat waves and extreme heat events. *Plant, Cell & Environment*. http://dx.doi.org/10.1111/pce.12417.
Trenberth, K. E., Fasullo, J. T., & Kiehl, J. (2009). Earth's global energy budget. *Bulletin of the American Meteorological Society*, *90*, 311–323.
Vicente-Serrano, S. M., Lopez-Moreno, J. I., Beguería, S., Lorenzo-Lacruz, J., Sanchez-Lorenzo, A., García-Ruiz, J. M., ... Espejo, F. (2014). Evidence of increasing drought severity caused by temperature rise in Southern Europe. *Environmental Research Letters*, *9*, 044001. http://dx.doi.org/10.1088/1748-9326/9/4/044001.
Vogelmann, J. E., Tolk, B., & Zhu, Z. (2009). Monitoring forest changes in the southwestern United States using multitemporal Landsat data. *Remote Sensing of Environment*, *113*, 1739–1748.
Wan, Z. (2008). New refinements and validation of the MODIS land-surface temperature/emissivity products. *Remote Sensing of Environment*, *112*, 59–74.
Wan, Z., & Dozier, J. (1989). Land-surface temperature measurement from space: Physical principles and inverse modeling. *IEEE Transactions on Geoscience and Remote Sensing*, *27*, 268–278.
Wan, Z., & Dozier, J. (1996). A generalized split-window algorithm for retrieving land-surface temperature from space. *IEEE Transactions on Geoscience and Remote Sensing*, *34*, 892–905. http://dx.doi.org/10.1109/36.508406.
Wan, Z., & Li, Z. L. (1997). A physics-based algorithm for retrieving land-surface emissivity and temperature from EOS/MODIS data. *IEEE Transactions on Geoscience and Remote Sensing*, *35*, 980–996.
Wan, Z., Wang, P., & Li, X. (2004). Using MODIS land surface temperature and normalized difference vegetation index products for monitoring drought in the southern great plains, USA. *International Journal of Remote Sensing*, *25*, 61–72.
Wan, Z., Zhang, Y., Zhang, Q., & Li, Z. -L. (2004). Quality assessment and validation of the MODIS global land surface temperature. *International Journal of Remote Sensing*, *25*, 261–274.
Waring, R. H. (1969 September 11–12). Matching Species to Site. In R. K. Herman (Ed.), *Proceedings of the symposium on regeneration of Ponderosa Pine*. Corvallis, Oregon: Oregon State University.
Westerling, A. L., Hidalgo, H. G., Cayan, D. R., & Swetnam, T. W. (2006). Warming and earlier spring increase western U.S. forest wildfire activity. *Science*, *313*, 940–943.
Williams, A. P., Allen, C. D., Macalady, A. K., Griffin, D., Woodhouse, C. A., Meko, D. M., ... McDowell, N. G. (2013). Temperature as a potent driver of regional forest drought stress and tree mortality. *Nature Climate Change*, *3*, 292–297.
Williams, M., Law, B. E., Anthoni, P. M., & Unsworth, M. H. (2001). Use of a simulation model and ecosystem flux data to examine carbon–water interactions in Ponderosa pine. *Tree Physiology*, *21*, 287–298.
Zhang, K., Kimball, J. S., Mu, Q. Z., Jones, L. A., Goetz, S. J., & Running, S. W. (2009). Satellite based analysis of northern ET trends and associated changes in the regional water balance from 1983 to 2005. *Journal of Hydrology*, *379*, 92–110.